Heliyon 10 (2024) e24983

Contents lists available at ScienceDirect

Heliyon

journal homepage: www.cell.com/heliyon

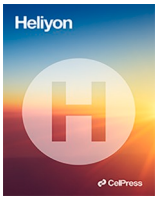

Research article

Altenusin, a fungal metabolite, alleviates TGF-β1-induced EMT in renal proximal tubular cells and renal fibrosis in unilateral ureteral obstruction

Natechanok Thipboonchoo [a], Somsak Fongsupa [b], Sanya Sureram [c], Suliporn Sa-nguansak [c], Chatchai Kesornpun [c], Prasat Kittakoop [c,d,e], Sunhapas Soodvilai [a,e,f,*]

[a] Research Center of Transport Protein for Medical Innovation, Department of Physiology, Faculty of Science, Mahidol University, Bangkok 10400, Thailand
[b] Department of Medical Technology, Faculty of Allied Health Science, Thammasat University Rangsit Campus, Thailand
[c] Chulabhorn Research Institute, Kamphaeng Phet 6 Road, Laksi, Bangkok 10210, Thailand
[d] Chulabhorn Graduate Institute, Program in Chemical Sciences, Chulabhorn Royal Academy, Laksi, Bangkok 10210, Thailand
[e] Center of Excellence on Environmental Health and Toxicology (EHT), OPS, Ministry of Higher Education, Science, Research and Innovation, Bangkok 10400, Thailand
[f] Excellent Center for Drug Discovery, Mahidol University, Bangkok 10400, Thailand

ARTICLE INFO

Keywords:
Chronic kidney disease
fibrosis
Renal proximal tubular cell
TGF-β1/Smad
Unilateral ureteral obstruction

ABSTRACT

Renal fibrosis is a pathological feature of chronic kidney disease (CKD), progressing toward end-stage kidney disease (ESKD). The aim of this study is to investigate the therapeutic potential of altenusin, a farnesoid X receptor (FXR) agonist derived from fungi, on renal fibrosis. The effect of altenusin was determined (i) *in vitro* using the transforming growth factor β1 (TGF-β1)-induced epithelial to mesenchymal transition (EMT) of human renal proximal tubular cells and (ii) *in vivo* using mouse unilateral ureteral obstruction (UUO). The findings revealed that incubation of 10 ng/ml TGF-β1 promotes morphological change in RPTEC/TERT1 cells, a human renal proximal tubular cell line, from epithelial to fibroblast-like cells. TGF-β1 markedly increased EMT markers namely α-smooth muscle actin (α-SMA), fibronectin, and matrix metalloproteinase 9 (MMP-9), while decreased the epithelial marker E-cadherin. Co-incubation TGF-β1 with altenusin preserved the epithelial characteristics of the renal epithelial cells by antagonizing TGF-β/Smad signaling pathway, specifically a decreased phosphorylation of Smad2/3 with an increased level of Smad7. Interestingly, the antagonizing effect of altenusin does not require FXR activation. Moreover, altenusin could reverse TGF-β1-induced fibroblast-like cells to epithelial-like cells. Treatment on UUO mice with 30 mg/kg altenusin significantly reduced the expression of α-SMA, fibronectin, and collagen type 1A1 (COL1A1). The reduction in the renal fibrosis markers is correlated with the decreased phosphorylation of Smad2/3 levels but does not improve E-cadherin protein expression. Collectively, altenusin reduces EMT in human renal proximal tubular cells and renal fibrosis by antagonizing the TGF-β/Smad signaling pathway.

* Corresponding author. Department of Physiology, Faculty of Science, Mahidol University, Bangkok 10400, Thailand.
E-mail address: Sunhapas.soo@mahidol.ac.th (S. Soodvilai).

https://doi.org/10.1016/j.heliyon.2024.e24983
Received 7 June 2023; Received in revised form 17 January 2024; Accepted 17 January 2024
Available online 19 January 2024

1. Introduction

Chronic kidney disease (CKD) refers to the progressive loss of kidney function, progressing toward end-stage kidney disease (ESKD) which requires kidney replacement therapy [1]. Renal fibrosis is the final common outcome of almost all kidney diseases and is strongly correlated with kidney insufficiency [2]. The current drugs for renal fibrosis and CKD have limited efficacies, they can only slow progression of the diseases, but they cannot stop or reverse the disease progression. Therefore, discovery of effective therapy for renal fibrosis and CKD is urgently needed [3]. Fibrosis is initiated by accumulated inflammation e.g., sustained activation of injurious stimuli which could lead to extracellular matrix (ECM) accumulation and epithelial-mesenchymal transition (EMT) of tubular epithelial cells [2]. The accumulation of ECM is augmented either by increased numbers of ECM-producing cells through the recruitment of myofibroblasts from other tissues, by the transformation of cells in the kidney into myofibroblasts such as endothelial to mesenchymal transition (EnMT), and/or by an increase in the EMT process [2]. During injury, kidneys secrete numerous cytokines and growth factors [4]. Among these, transforming growth factor β1 (TGF-β) is a potent and well-known stimulus of the EMT process and subsequently causes fibrosis [5]. TGF-β upregulates fibrotic genes including α-smooth muscle actin (α-SMA), vimentin, collagen, and fibronectin while downregulating E-cadherin expression. TGF-β1 regulates the proteins involved in fibrosis via two signaling pathways including the suppressor of mothers against decapentaplegic (Smad) and the non-Smad pathways [6–8]. TGF-β-Smad signaling is activated by the binding of active TGF-β1 to TGF-β receptor type II (TβRII), causing heterodimerization in TβRII and TβRI [6,9,10]. TβR is the serine-threonine kinase receptor, which once dimerized can phosphorylate downstream signaling protein Smad2 and Smad3 [6,9,10]. Phosphorylated (p)-Smad2 and *p*-Smad3 form complexes with Smad4 which get into the nucleus and act as transcription factors [6,9,10]. Phosphorylation of Smad2 and Smad3 is negatively regulated by Smad7 via direct interference with the phosphorylation process or downregulating TβRI [6,9,10]. For TGF-β-non-Smad signaling pathways, p-extracellular signal-regulated kinase 1/2 (*p*-ERK1/2), p-c-Jun N-terminal kinase (*p*-JNK), and p-p38 are upregulated upon TGF-β activation [6,11].

As a nuclear receptor subfamily member, the farnesoid X receptor (FXR) plays a crucial role in bile acid, glucose, and lipid metabolism [12]. The FXR can be activated by endogenous and exogenous ligands such as chenodeoxycholic acid (CDCA), cholic acid (CA), lithocholic acid (LCA), deoxycholic acid (DCA), obeticholic acid (OCA), and GW4064 [13,14]. In the kidneys, the FXR mRNA and protein expression were found to be decreased in patients with diabetes- and obesity-related kidney disease [15]. Targeting FXR activation has been found to preserve the kidney function of diabetic nephropathy rodent models [15,16]. Moreover, FXR agonists have suppressed renal fibrosis in mouse unilateral ureteral obstruction (UUO) model of renal fibrosis [17]. Interestingly, activation of the FXR has alleviated liver fibrosis through the suppression of TGF-β mRNA and protein expressions [18,19]. Moreover, the treatment of OCA protects against lung fibrosis by decreasing TGF-β mRNA expression [20]. Accordingly, targeting FXR activation and TGF-β suppression may be a promising option for fibrosis therapy in kidney disease.

Altenusin is a nonsteroidal microbial metabolite derived from fungi (Alternaria sp.) [21–24]. Numerous biological activities of altenusin have been reported. Altenusin displays neuroprotective effects against oxidative damage by acting as a potent nuclear factor-erythroid derived 2-like 2 (Nrf2) activator in PC12 cells [25]. In addition, altenusin has shown anti-diabetic properties by inhibiting α-glucosidase and pancreatic lipase enzymes [26]. Recently, altenusin has been identified as a selective FXR agonist [27]. Treatment with altenusin in a mouse model of nonalcoholic fatty liver disease (NAFLD) was found to alleviate disease progression [27]. However, there is still no reports whether altenusin can prevent or reverse TGFβ1-induced EMT of renal proximal tubular cells and attenuate renal fibrosis in animal models. The present study investigates the therapeutic potential of altenusin on TGF-β1-indeced EMT in human renal proximal tubular cells and in murine model of renal fibrosis. Here, we firstly reported that altenusin prevented and reversed TGF-β1-induced EMT in human renal proximal tubular cells and alleviated renal fibrosis in UUO mice.

2. Materials and methods

2.1. Chemicals

The TGF-β1 (7754-BH-005) was purchased from R&D Systems (MN, USA). Primary antibodies including *p*-Smad2 (18338S), total-Smad2 (5339S), *p*-Smad3 (9520S), total-Smad3 (9523S), E-cadherin (3195S), matrix metalloproteinase 9 (MMP-9) (13667T), and glyceraldehyde-3-phosphate dehydrogenase (GAPDH) (2118S) were obtained from cell signaling (MA, USA). Smad7 (sc-365846), TβR1 (sc-398), fibronectin (sc-8422), COL1A1 (sc-293182), and anti-neutrophil gelatinase-associated lipocalin (NGAL) (sc-515876) antibodies were purchased from Santa Cruz Biotechnology (CA, USA) and α-SMA (ab5694) primary antibodies from Abcam (MA, USA). The GW4064 (G5172) was purchased from Sigma Aldrich (DE, USA.), and DY268 (5656) was obtained from Tocris Bioscience (MN, USA). All other chemicals were analytical grade and purchased from commercial sources.

2.2. Altenusin isolation

The endophytic fungus *Alternaria destruens* PobtRO-6, isolated from a plant leaf of *Plumeria obtuse*, was cultivated in rice medium. *A. destruens* PobtRO-6 was grown in 1L-Erlenmeyer flask (50 flasks) under static conditions at room temperature for 30 days. The fungal culture was extracted with an equal volume of ethyl acetate. The extract was evaporated by a rotary evaporator to yield approximately 55.0 g of a crude extract. The crude extract was then purified through Sephadex-LH20 column chromatography and eluted with ethanol. Each fraction was evaporated by a rotary evaporator. Altenusin (50.8 g) was obtained from fractions 12–16. Residual solvent was removed by vacuum drying under reduced pressure. ^{1}H NMR analysis of the purified altenusin revealed >95 % purity.

2.3. Cell culture

The renal proximal tubular (RPTEC/TERT1) cell line was purchased from American Type Culture Collection (VA, USA). Cells were grown in Dulbecco's Modified Eagle Medium/Nutrient Mixture F-12 (DMEM/F12) medium supplemented with 100 U/mL penicillin, 100 μg/mL streptomycin, 5 μg/mL insulin, 5 ng/mL sodium selenite, 5 μg/mL transferrin, 10 ng/mL epithelial growth factor, and 36 ng/mL hydrocortisone at 37 °C, 80 % humanify, and 5 % CO_2. The cells were grown until they matured and then treated under various conditions.

2.4. Nuclear protein isolation and treatment protocol

Nuclear and cytosol proteins were extracted according to NE-PER™ Nuclear and Cytoplasmic Extraction Reagents (Cat no. 78833, Thermo Fisher Scientific Inc., MA, USA). Briefly, mature RPTEC/TERT1 cells were trypsinized with 0.25 % trypsin EDTA and centrifuged at 500×*g* for 5 min. Cells were washed and resuspended in phosphate buffer saline (PBS). The Cytoplasmic Extraction Reagent I (CER I) was added to the cell pellets, vortexed vigorously, and incubated on ice for 10 min. The Cytoplasmic Extraction Reagent II (CER II) was added, vortexed, and incubated on ice for 1 min. Cell lysates were centrifuged at 16000×*g* for 5 min. Cytosol lysates were immediately transferred to the clean pre-chilled tubes. For nuclear protein extraction, insoluble cell pellets containing nuclei were added with ice-cold Nuclear Extraction Reagent (NER) and vortexed every 10 min for 40 min. The NER with nuclei was then centrifuged at 16000×*g* for 10 min, and the nuclear extract was immediately moved to clean the pre-chilled tube. All samples were stored at −80 °C until use.

2.5. Mouse UUO model

The animal study (protocol number: MUSC64-036-585) was approved by the Faculty of Science, Mahidol University–Institutional Animal Care and Use Committee (MUSC–IACUC). Male C57BL/6 mice (seven weeks, 20–25 g) were purchased from Nomura Siam International Co, Ltd (Bangkok, Thailand). The mice were acclimatized for a week under 12:12 h light-dark cycle, room temperature of 22–24 °C, and 50–60 % relative humidity. The mice were fed a normal diet and water ad libitum. After the acclimatization period, the animals were randomly divided into four groups: sham-operated (S), UUO-operated (U), UUO plus 3 mg/kg i.p. altenusin (U + L), and UUO plus 30 mg/kg i.p. altenusin (U + H). The UUO operation was performed as described in the previous study [28]. Briefly, the mice were anesthetized with isoflurane, and the left ureter was then separated and ligated with silk sutures. The sham group underwent the same procedure, and the left ureter was exposed without ligation. Post modeling completion, the mice were administered with treatment or equal volumes of a vehicle by intraperitoneal injection. After treatment for 14 days, the mice were weighed and euthanized.

2.6. Western blot analysis

The proteins of RPTEC/TERT1 cells and mouse kidneys were extracted using RIPA buffer. The lysis buffer containing digested components was centrifuged at 12,000 rpm at 4 °C for 20 min and the supernatant proteins were collected. Equal amounts of proteins were denatured for 5 min at 95 °C, separated by 10 or 12 % acrylamide sodium dodecyl sulfate polyacrylamide gel electrophoresis (SDS-PAGE), and then transferred onto 0.45-μm nitrocellulose membranes (Bio-Rad, CA, USA). Membranes were blocked by a 5 % blotting grade blocker (Bio-Rad, CA, USA) for 1 h and then incubated overnight with antibodies. After the primary incubation period, the membranes were washed three times using Tris-buffered saline with 0.1 % Tween 20 (TBST) and incubated with a horseradish peroxidase-conjugated secondary antibody. The immune complexes were detected using the Electro-Chemi-Luminescence (ECL) system and visualized by Azure 600 Gel Imaging System (Azure Biosystem, Inc., CA, USA). The intensity of the bands was quantified using ImageJ software. Data were shown as the ratio of densitometry in interested proteins normalized by loading the control protein (GAPDH) and relative expression or relative sham.

2.7. Examination of kidney injury and fibrosis scoring

The kidney specimens were fixed in 4 % paraformaldehyde. Kidney sections measuring 5 μm were stained with hematoxylin and eosin (H&E) and Masson trichome to obtain the injury score and trichome positive area, respectively. Kidney injury features included necrotic tubular cells, sclerosis, tubular dilation, and inflammatory cells. Abnormal areas were evaluated using a blind test with a score of 0 = normal, 1 = mild (<25 %, abnormal pathological injury), 2 = moderate (25–50 %), 3 = severe (50–75 %), and 4 = large area injury (>75 %). The percentage of the Masson trichome positive area was scored [29]. The mean score was calculated by counting 10 different fields for each sample. Semi-quantitative evaluation and the histopathological scoring of tissue damage and fibrosis were carried out and graded by pathologists.

2.8. Statistical analysis

The results of all experiments were expressed as mean ± SD using GraphPad Prism for Windows (CA, USA). All data were analyzed using one-way analysis of variance (ANOVA) followed by Tukey's Multiple Comparison Test. The level of significance for the statistical test was accepted at $p < 0.05$.

3. Results

3.1. Altenusin prevents TGF-β1-induced EMT in human renal proximal tubular cells

To investigate the protective effect of altenusin in TGF-β1-induced EMT on renal proximal tubular cells, mature RPTEC/TERT1 cells were incubated with vehicle control, 10 ng/ml TGF-β1 alone and in combination with an altenusin concentration of 10–100 μM for 48 h (Fig. 1A). TGF-β1-induced cell morphology changed from epithelium to a fibroblast-like structure. Co-incubation with altenusin demonstrated a protective effect from morphology transformation by TGF-β1 treatment in a concentration-dependent manner. In comparison to the vehicle-treated cells, the cells incubated with TGF-β1 showed significantly reduced E-cadherin expression and the expression levels of α-SMA, fibronectin, and MMP-9 were dramatically increased. Co-incubating the cells with TGF-β1 and altenusin significantly prevented E-cadherin reduction while significantly reducing fibronectin, α-SMA, and MMP-9 expression induced by TGF-β1 (Fig. 1B).

3.2. Altenusin alleviates EMT in renal proximal tubular cells by antagonizing the TGF-β Smad signaling pathway

To prove whether altenusin prevents EMT in renal proximal tubular cells through inhibition of the TGF-β signaling pathway, the effect of altenusin was determined on the signaling proteins of TGF-β. As shown in Fig. 2, treating the cells with 10 ng/ml TGF-β1 for 48 h dramatically increased the levels of *p*-Smad2 and *p*-Smad3 in the downstream signaling of TGF-β1. Altenusin significantly decreased the levels of *p*-Smad2 and *p*-Smad3 induced by TGF-β1 in a concentration-dependent manner (Fig. 2A). In contrast to *p*-Smad2 and *p*-Smad3, altenusin significantly increased the expression of Smad7 (Fig. 2A). Interestingly, the TGF-β1-induced increase in TβR1 expression was attenuated by altenusin (Fig. 2A). Altenusin has been identified as a specific FXR agonist [27]. The involvement of FXR on the beneficial effect of altenusin was further determined. Results showed that altenusin and GW4064 (an FXR agonist) likely preserved E-cadherin protein expression in comparison to TGF-β1 (Fig. 2B). Co-incubation with DY268, an FXR antagonist, did not reduce the effect of altenusin or GW4064 on E-cadherin expression (Fig. 2B). Altenusin reduced α-SMA protein expression whereas GW4064 did not (Fig. 2B). Co-treatment of altenusin with DY268 under the condition of TGF-β1 did not attenuate the effect of altenusin on α-SMA protein expression. Interestingly, DY268 did not withdraw the effect of altenusin and GW4064 on fibronectin expression. In addition, DY268 had no effect on altenusin reduction in *p*-Smad2 and *p*-Smad3 levels. GW4064 significantly reduced *p*-Smad2 level whereas it tended to reduce *p*-Smad3 level. Co-treatment of GW4064 with DY268 did not attenuate these effects. The results implied that the anti-EMT effect of altenusin did not require FXR activation.

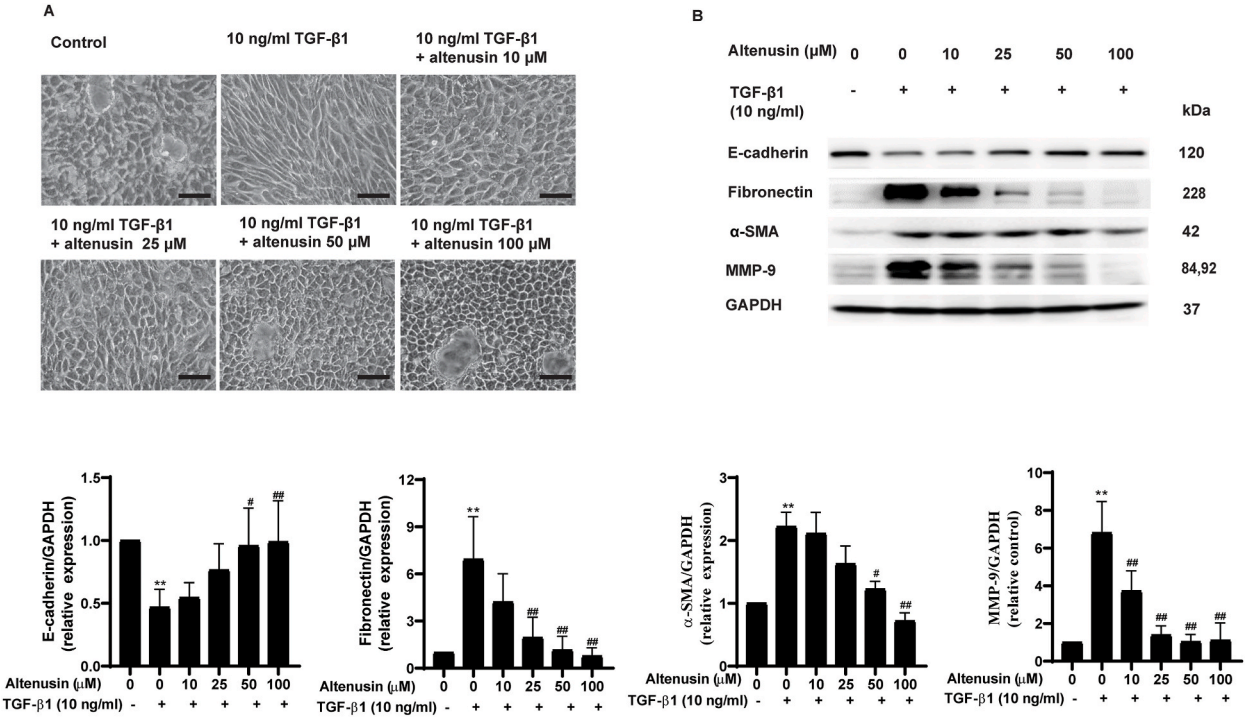

Fig. 1. Effect of altenusin on TGF-β1-induced EMT in human renal proximal tubular cells (A) Morphology of RPTEC/TERT1 cells following 48 h incubation of the control, 10 ng/ml TGF-β1, and 10 ng/ml TGF-β1 plus altenusin (10–100 μM) (200X, scale bar = 50 μm). (B) The representative immunoblots and protein intensities of E-cadherin, α-SMA, fibronectin, and MMP-9 (non-adjusted images S1). Data are shown as mean ± SD from five independent experiments (*$p < 0.05$ and **$p < 0.01$ vs control, $^{\#}p < 0.05$ and $^{\#\#}p < 0.01$ vs 10 ng/ml TGF-β1).

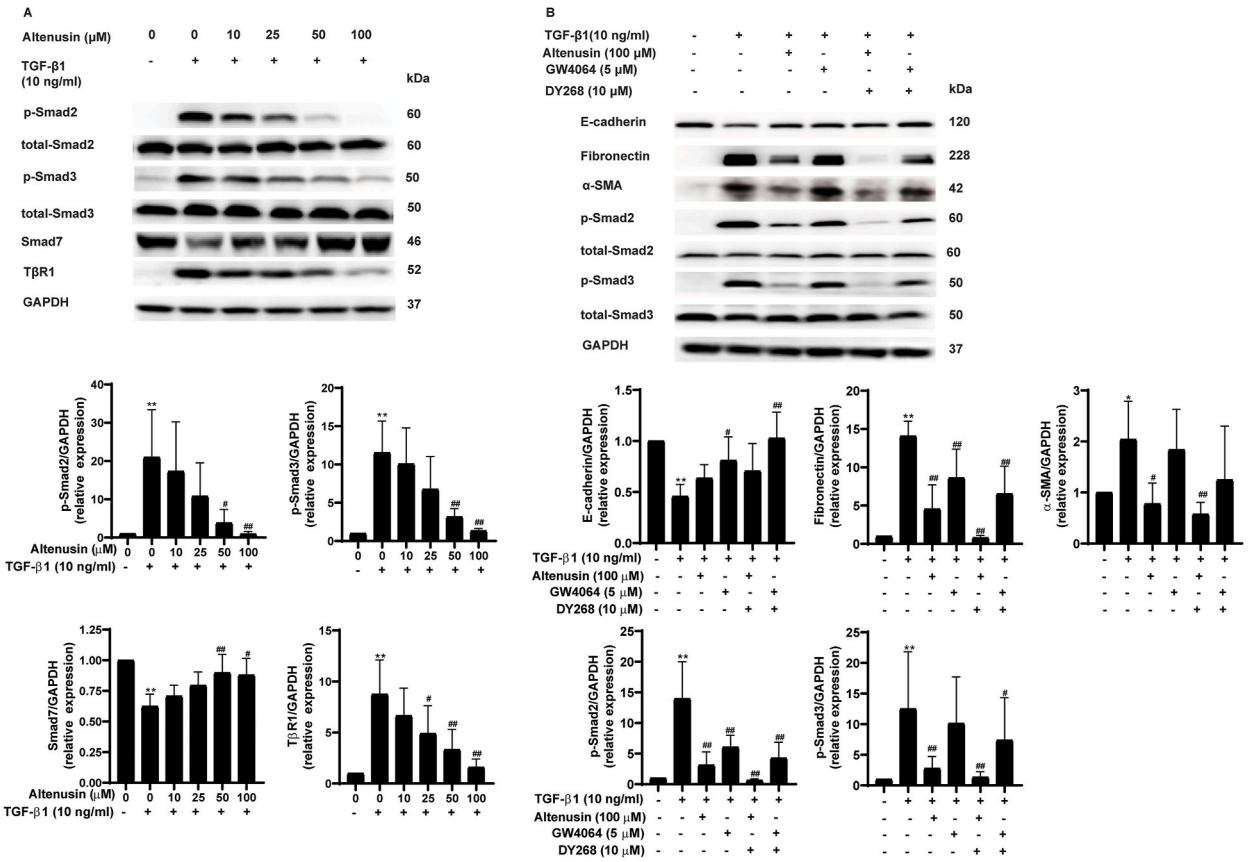

Fig. 2. Effect of altenusin on the TGF-β signaling pathway (A) The representative immunoblots and intensities of Smad2, Smad3, Smad7, and TβR1 proteins following 48 h incubation of the vehicle, 10 ng/ml TGF-β1, and 10 ng/ml TGF-β1 plus altenusin (10–100 μM). (B) The representative immunoblots and intensities of E-cadherin, fibronectin, α-SMA, *p*-Smad2, total-Smad2, *p*-Smad3, and total-Smad3 proteins following 48 h of treatment (non-adjusted images S2). Data are shown as mean ± SD from five independent experiments ($^{*}p < 0.05$ and $^{**}p < 0.01$ vs control, $^{\#}p < 0.05$ and $^{\#\#}p < 0.01$ vs 10 ng/ml TGF-β1).

3.3. Altenusin reduces the nuclear localization of p-Smad2 and p-Smad3 during TGF-β1 treatment

To regulate gene transcription, a complex of *p*-Smad2, *p*-Smad3, and Smad4 needs to be translocated into the nucleus [6]. Therefore, the effect of altenusin on the nuclear localization of *p*-Smad2 and *p*-Samd3 induced by TGF-β1 was determined. As shown in Fig. 3 (A-B), *p*-Smad2 and *p*-Smad3 levels in the nuclear compartment were significantly increased with the treatment of 10 ng/ml TGF-β1 in comparison to the control. Altenusin dramatically reduced the *p*-Smad2 and *p*-Smad3 levels in the nuclear compartment when compared to those in the TGF-β1-treated cells.

3.4. Acute effect of altenusin on TGF-β1-induced p-Smad2 and p-Smad3 phosphorylation

Reduced phosphorylation of Smad2 and Smad3 by altenusin is correlated with increased Smad7 and decreased TβR1 protein expression levels. To test whether the effect of altenusin on *p*-Smad2 and *p*-Smad3 was mediated by the modulation of Smad7 and TβR1, the acute effect of altenusin at 100 μM on *p*-Smad2 and *p*-Smad3 induced by TGF-β was determined. As shown in Fig. 4 (A-B), the incubation of cells with TGF-β1 for 30 and 60 min increased the phosphorylation levels of both Smad2 and Smad3. Co-incubation with altenusin led to a decrease in *p*-Smad2 and *p*-Smad3 levels without altering the expression of either Smad7 or TβR1. These results implied that the effect of altenusin on Smad2 and Smad3 phosphorylation did not require an increased Smad7 expression and a decreased TβR1 expression in the early phase of TGF-β1 induction.

3.5. Altenusin reverses TGF-β1-induced EMT in renal proximal tubular cells

To prove whether altenusin could reverse the effect of TGF-β1-induced EMT in proximal tubular cells, the fibroblast cells were firstly induced by TGF-β1 for 24 h, then further incubated for 48 h with TGF-β1 or TGF-β1 plus altenusin. As shown in Fig. 5 (A-C), co-treatment with altenusin could reverse the fibroblast-like structure into an epithelial-like structure. As expected, the co-incubation of

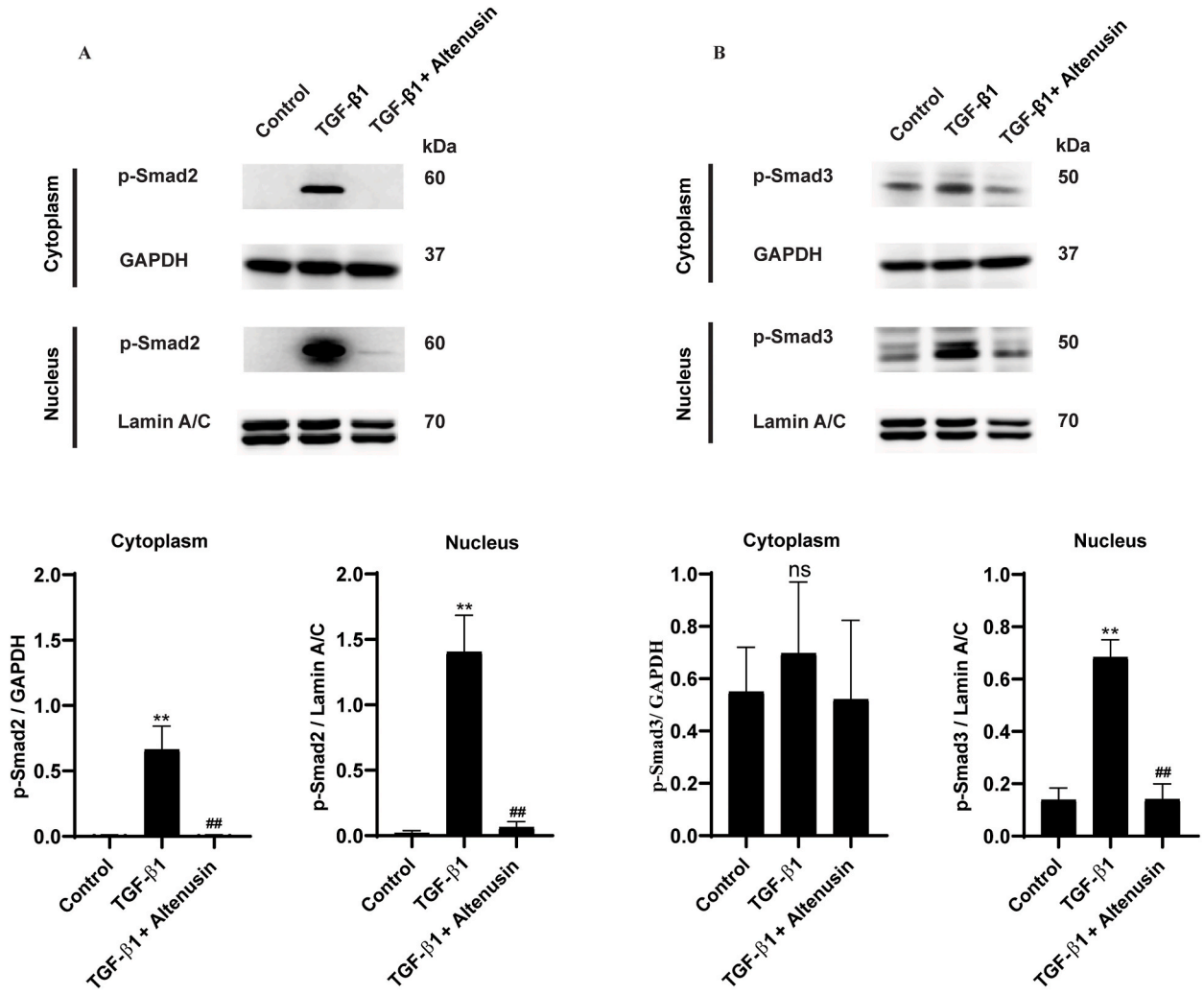

Fig. 3. Effect of altenusin on the TGF-β1-induced nuclear localization of Smad2 and Smad3 The representative immunoblots (non-adjusted images S3) and intensities of nuclear and cytosol protein of *p*-Smad2 (A) and *p*-Smad3 (B) following 48 h of incubation with the vehicle, 10 ng/ml TGF-β1 alone, and TGF-β1 plus 100 μM altenusin. Data are shown as mean ± SD from three independent experiments (**$p < 0.01$ vs control, $^{\#\#}p < 0.01$ vs 10 ng/ml TGF-β1, ns = non-significant vs control).

altenusin significantly increased E-cadherin whereas altenusin decreased α-SMA and fibronectin protein expression, with a reduction in *p*-Smad2, and *p*-Smad3 levels.

3.6. Effect of altenusin on fibrosis and injury in the kidneys of UUO mice

To determine whether altenusin retarded fibrosis in the kidneys of UUO mice, the Masson trichome staining was used and expression of fibrosis markers were determined. As shown in Fig. 6A, UUO significantly increased the percentage of the positive area in the kidneys compared with the sham operation. Treatment of altenusin (30 mg/kg) reduced the positive area of Masson trichome staining compared to that in UUO. Whereas altenusin (3 mg/kg) slightly reduced the positive area of Masson trichome staining. UUO treated with the vehicle showed significant increase in the expression levels of fibronectin, α-SMA, and COL1A1 in comparison to those in the sham (Fig. 6B). The inductions of these proteins were attenuated by treatment with 30 mg/kg altenusin. Interestingly, altenusin did not improve E-cadherin protein expression. Next, we investigated whether altenusin reduced fibrosis through the TGF-β/Smad signaling pathway by examining the effect of altenusin on Smad expression. UUO increased the kidney phosphorylation level of *p*-Smad2 and *p*-Smad3 (Fig. 7 (A-B)). Treatment with altenusin (30 mg/kg) significantly reduced both *p*-Smad2 and *p*-Smad3 levels. In addition to kidney fibrosis, the effect of altenusin on kidney injury induced by UUO was determined. As shown in Fig. 8, UUO dramatically increased kidney injury as indicated by the kidney injury score (Fig. 8A) and increase in NGAL expression (Fig. 8B). Treatment with altenusin did not reduce the kidney injury score and NGAL expression.

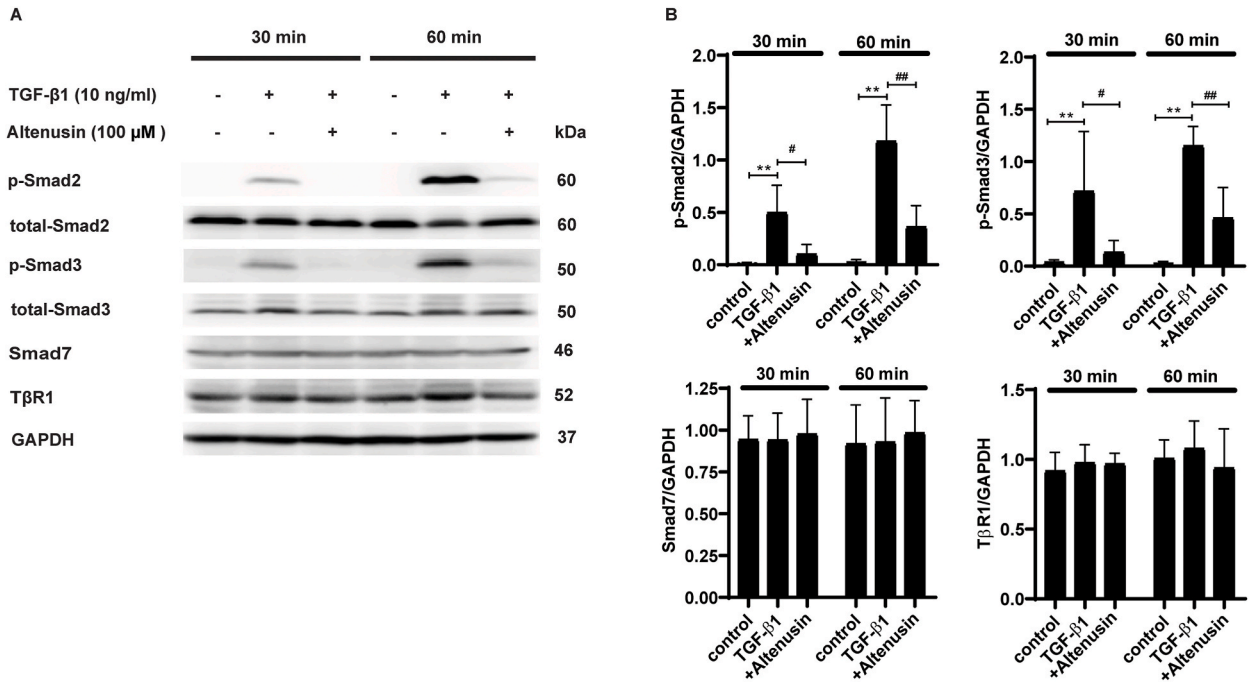

Fig. 4. Acute effect of altenusin on TGF-β1-induced phosphorylation of Smad2 and Smad3 in renal proximal tubular cells The representative (A) immunoblots (non-adjusted images S4) and (B) protein intensities of *p*-Smad2, *p*-Smad3, Smad7, and TβR1 following 30 and 60 min of incubation. Data are shown as mean ± SD from four independent experiments ($^{*}p < 0.05$ and $^{*}p < 0.01$ vs control, $^{\#}p < 0.05$ and $^{\#\#}p < 0.01$ vs 10 ng/ml TGF-β1).

4. Discussion

Kidney fibrosis is the outcome of the most CKD and correlates with a reduction in kidney function. Unfortunately, the efficacy of current therapies is limited; therefore, the development of an effective regimen for treating kidney fibrosis is necessary. In this study, the researchers first demonstrated that altenusin, a biphenyl phenolic compound derived from fungi [27,30], alleviates TGF-β1-induced EMT in human renal proximal tubular cells and kidney fibrosis in UUO mice.

TGF-β1 plays an important role in EMT and kidney fibrosis [31]. The upregulation of EMT and fibrosis markers can be found under the activation of TGF-β1 through its downstream signaling pathways [7,32]. TGF-β1-induced morphology changes the renal proximal tubular cells into a fibroblast-like structure representing EMT [7]. The findings of this study reveal that altenusin can prevent and reverse TGF-β1-induced EMT in renal proximal tubular cells. TGF-β1 induced fibroblast characteristics by increasing the fibroblast markers i.e., fibronectin and α-SMA, while reducing E-cadherin, an epithelial marker [7,33]. In addition to the EMT markers, MMP-9 (an enzyme responsible for the initiation and progression of kidney fibrosis) [34] was upregulated in the presence of TGF-β1. Altenusin extensively reduced MMP-9 protein expression induced by TGF-β1, implying that altenusin not only inhibits EMT but also reduces fibrosis in renal proximal tubular cells. Mechanically, TGF-β1 induced EMT in renal proximal tubular cells and fibrosis via the activation of Smads [6]. Altenusin treatment dramatically reduced the phosphorylation level of Smad2/3 while increasing Smad7 expression. These results suggest that the inhibitory effect of altenusin on EMT is mediated by altering the Smad signaling pathway. Smad7 is a negative regulator of Smad2/3 via the down-regulation of TβR1 protein [6]. It is interesting whether the inhibitory effect of altenusin on *p*-Smad2/3 represented a downstream increase in Smad7 expression or was mediated by the direct inhibition of altenusin in the Smad2/3 phosphorylation process. The phosphorylation process of Smad2/3 induced by TGF-β1 occurred in 1 h [35]. In this study, we demonstrated that altenusin can reduce the phosphorylation levels of Smad2/3 upon TGF-β activation in minutes without changing the Smad7 and TβR1 protein expression. This evidence implies that, in the early phase of TGF-β1/TβR1 activation, the inhibitory effect of altenusin on phosphorylation of Smad2/3 did not require alteration of Smad7 and TβR1 expression. The upregulation of Smad7 expression might contribute to the inhibitory effect of altenusin on Smad2/3 phosphorylation in a later phase of TGF-β1/TβR1 activation. Activated Smad2/3 (*p*-Smad2/3) formed a complex with Smad4 then translocated from cytosol into the nucleus in order to activate the target genes [9]. The results of this study reveal that altenusin can reduce the phosphorylation of Smad2/3 both in the nuclear compartment and the cytosol. These results imply that altenusin might reduce the *p*-Smad2/3 level in cytosol, resulting in a reduction in the nuclear compartment rather than inhibition of the *p*-Smad2/3 translocation process.

To be certain that the inhibitory of altenusin on fibrosis in cultured renal proximal tubular cells can be found *in vivo*, the effect of the compound was investigated in UUO mice which are widely used in the investigation of tubulointerstitial fibrosis [36]. UUO increased the positive area of Masson trichome staining as previously reported [29]. However, the degree of fibrosis in the present study was not as high as expected. The fibrosis area tended to reduce with altenusin treatment which might be caused by the mild fibrosis degree of

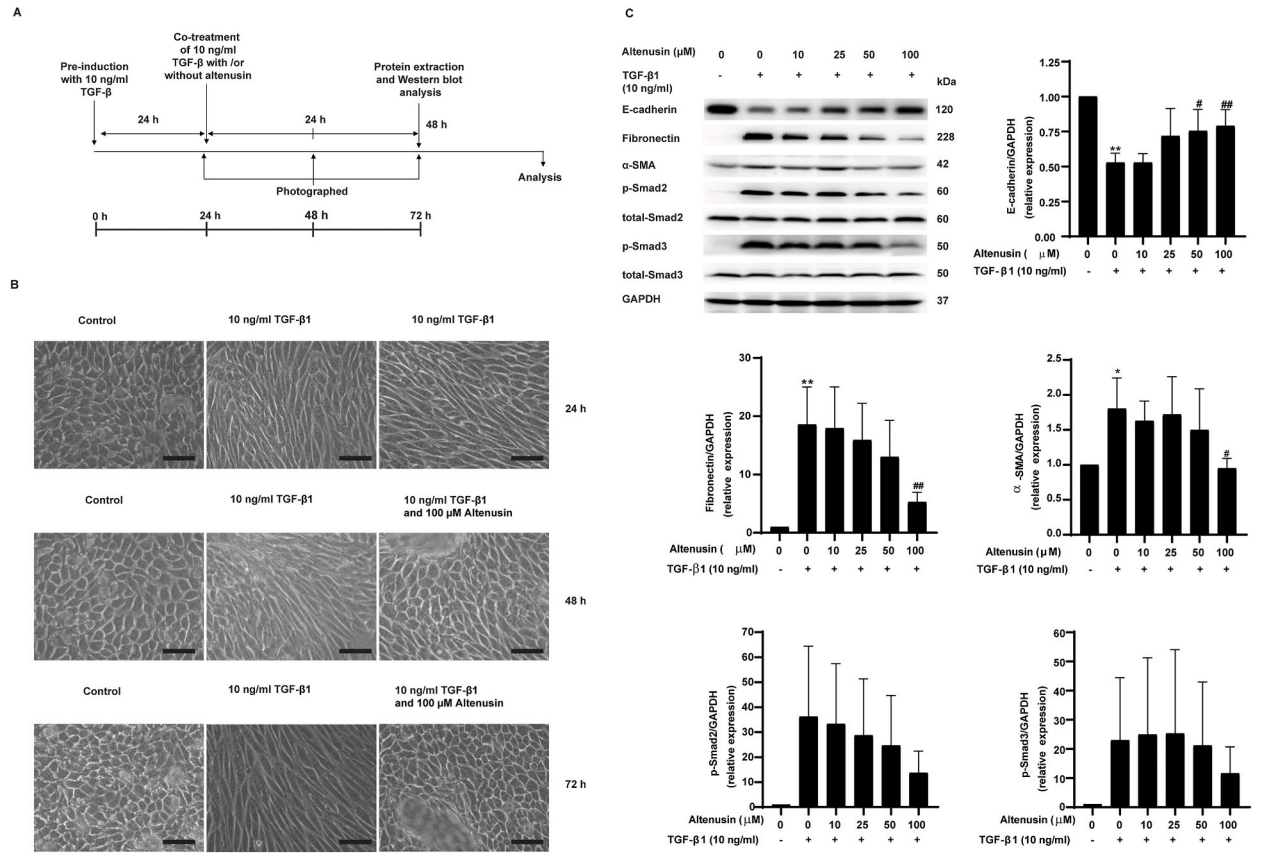

Fig. 5. Altenusin reverses TGF-β1-induced EMT in renal proximal tubular cells (A) Treatment protocol for examining the effect of altenusin on reversed TGF-β1-induced EMT in renal proximal tubular cells. (B) The representative image of renal proximal tubular cell morphology (200X, scale bar 50 μm). (C) The representative immunoblots and intensities of E-cadherin, α-SMA, fibronectin, and *p*-Smad2 and *p*-Smad3 proteins (non-adjusted images S5). Data are shown as mean ± SD from five independent experiments ($^{*}p < 0.05$ and $^{**}p < 0.01$ vs control, $^{\#}p < 0.05$ and $^{\#\#}p < 0.01$ vs 10 ng/ml TGF-β1).

the UUO mice. However, the UUO dramatically decreased E-cadherin while increasing fibronectin, COL1A1, and α-SMA protein expression which are the fibrotic markers [29]. Interestingly, treatment with altenusin (30 mg/kg) alleviated fibrosis by reducing fibronectin, COL1A1, and α-SMA expression but did not significantly improve E-cadherin protein expression. These results might imply that the beneficial effect of altenusin on renal fibrosis was selective. Since the TGF-β1 signaling pathway was under activation in the UUO model [37], we further investigated whether altenusin could reduce the activation of Smad2/3 in UUO-induced renal fibrosis. In the present study, the phosphorylation levels of Smad2/3, an activated Smad2/3, were increased in the UUO group, correlating well with the previous study [7]. The activation of Smad2/3 was attenuated by treatment with altenusin. These results suggest that altenusin alleviates kidney fibrosis in UUO mice via modulation of the TGF-β1-Smad signaling pathway. Pathogenesis of the fibrotic kidney in the UUO mouse model represents injury-induced renal fibrosis [37,38]. We then investigated whether the beneficial effect of altenusin on renal fibrosis was mediated by the inhibition of injury-induced renal fibrosis. As indicated by the results, UUO dramatically induced kidney injury as supported by an increase in kidney injury score and kidney NGAL expression, a kidney injury protein marker [39,40]. Interestingly, altenusin treatment did not significantly reduce the kidney injury score and renal NGAL expression. These results indicate that the inhibitory effect of altenusin on renal fibrosis is not targeted as a process of injury-induced renal fibrosis. In summary, the present study demonstrates the novel therapeutic potential of altenusin on TGF-β1-induced EMT in human renal proximal tubular cells and renal fibrosis in the UUO mouse model by antagonized TGF-β1/Smad signaling pathway.

Data availability statement

Data will be made available on request.

Additional information

No additional information is available for this paper.

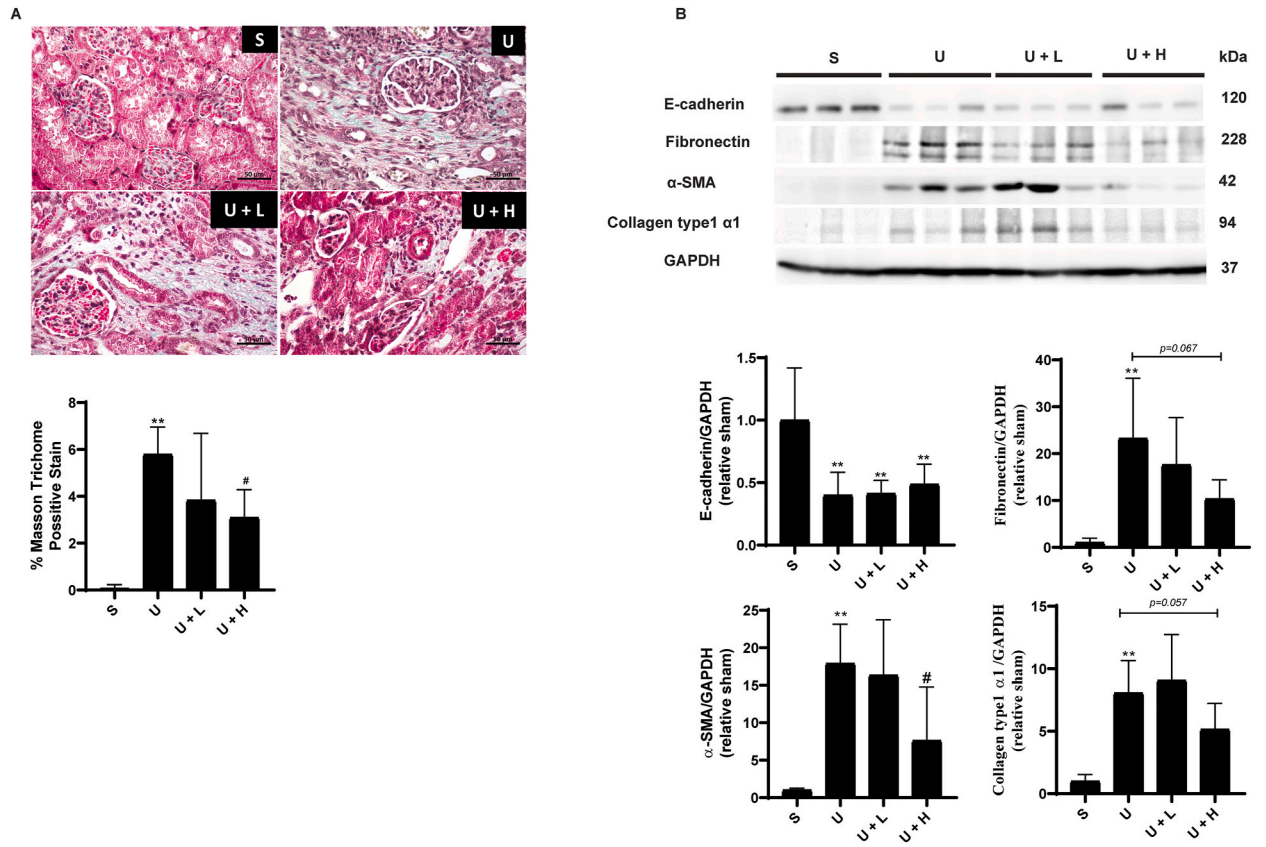

Fig. 6. Effect of altenusin on kidney fibrosis in UUO mice (A) The representative pictures (400X, scale bar 50 μm) and percentage Masson trichome staining of the sham (S), UUO (U), UUO + 3 mg/kg altenusin (U + L), and UUO + 30 mg/kg altenusin (U + H). (B) The representative immunoblots and intensity of fibronectin, α-SMA, collagen type 1 α 1, and E-cadherin proteins (non-adjusted images S6). Data are shown as mean ± SD of six mice (**$p < 0.01$vs sham and $^{\#}p < 0.05$ vs UUO).

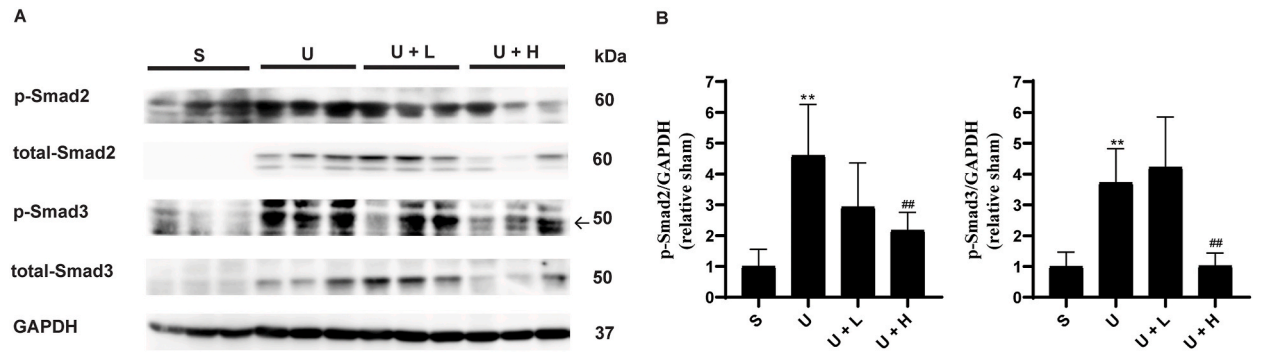

Fig. 7. Effect of altenusin on the TGF-β-Smad signaling pathway in UUO mice (A) The representative immunoblots of *p*-Smad2, total-Smad2, *p*-Smad3 total-Smad3, and GAPDH proteins of sham (S), UUO (U), UUO + 3 mg/kg altenusin (U + L), and UUO + 30 mg/kg altenusin (U + H) (non-adjusted images S7). (B) The representative intensity of indicated proteins. Data are shown as mean ± SD of six mice (**$p < 0.01$ vs sham and $^{\#\#}p < 0.01$ vs UUO).

Declaration of competing interest

The authors declare that they have no known competing financial interests or personal relationships that could have appeared to influence the work reported in this paper.

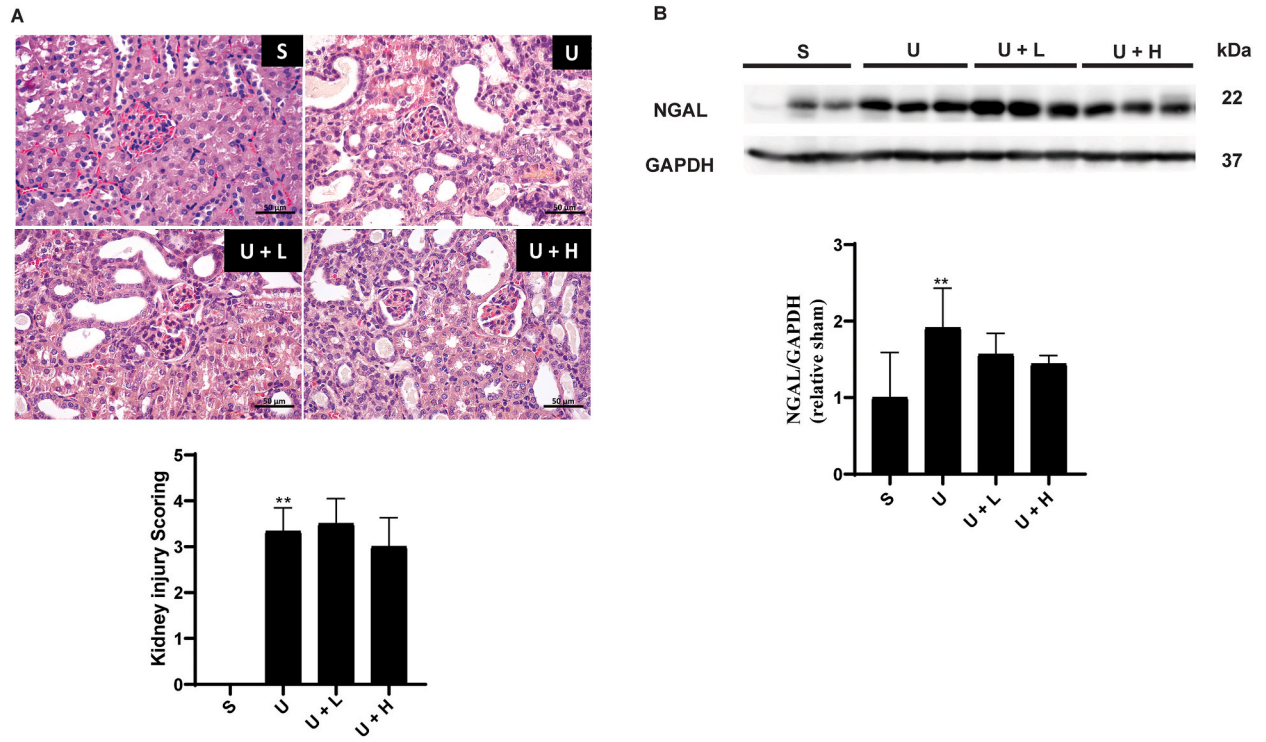

Fig. 8. Effect of altenusin on kidney injury in UUO mice (A) The representative pictures (400X, scale bar 50 μm) and kidney injury scoring of the sham (S), UUO (U), UUO + 3 mg/kg altenusin (U + L), and UUO + 30 mg/kg altenusin (U + H). (B) The representative immunoblots and intensity of NGAL protein (non-adjusted images S8). Data are shown as mean ± SD from six mice (**$p < 0.01$ vs sham).

Acknowledgment

This research project is supported by Mahidol University (Fundamental Fund: fiscal year 2023 by National Science Research and Innovation Fund (NSRF), Grant No. FF-062/2566). N.T. is supported by the Science Achievement Scholarship of Thailand (SAST). S. Sureram is supported by Thailand Science Research and Innovation (TSRI), Chulabhorn Research Institute, Grant No. 36824/4274394).

Appendix A. Supplementary data

Supplementary data to this article can be found online at https://doi.org/10.1016/j.heliyon.2024.e24983.

References

[1] C.P. Kovesdy, Epidemiology of chronic kidney disease: an update 2022, Kidney Int. Suppl. 12 (1) (2022) 7–11, https://doi.org/10.1016/j.kisu.2021.11.003.
[2] Y. Liu, Cellular and molecular mechanisms of renal fibrosis, Nat. Rev. Nephrol. 7 (12) (2011) 684–696, https://doi.org/10.1038/nrneph.2011.149.
[3] B.M. Klinkhammer, R. Goldschmeding, J. Floege, P. Boor, Treatment of renal fibrosis—turning challenges into opportunities, Adv. Chron. Kidney Dis. 24 (2) (2017) 117–129, https://doi.org/10.1053/j.ackd.2016.11.002.
[4] L. Gewin, R. Zent, A. Pozzi, Progression of chronic kidney disease: too much cellular talk causes damage, Kidney Int. 91 (3) (2017) 552–560, https://doi.org/10.1016/j.kint.2016.08.025.
[5] G. Vega, S. Alarcón, R. San Martín, The cellular and signalling alterations conducted by TGF-β contributing to renal fibrosis, Cytokine 88 (2016) 115–125, https://doi.org/10.1016/j.cyto.2016.08.019.
[6] A. Sureshbabu, S.A. Muhsin, M.E. Choi, TGF-β signaling in the kidney: profibrotic and protective effects, Am. J. Physiol. Ren. Physiol. 310 (7) (2016) F596–F606, https://doi.org/10.1152/ajprenal.00365.2015.
[7] X.-q. Geng, A. Ma, J.-z. He, L. Wang, Y.-l. Jia, G.-y. Shao, M. Li, H. Zhou, S.-q. Lin, J.-h. Ran, Ganoderic acid hinders renal fibrosis via suppressing the TGF-β/Smad and MAPK signaling pathways, Acta Pharmacol. Sin. 41 (5) (2020) 670–677, https://doi.org/10.1038/s41401-019-0324-7.
[8] R. Li, Y. Guo, Y. Zhang, X. Zhang, L. Zhu, T. Yan, Salidroside ameliorates renal interstitial fibrosis by inhibiting the TLR4/NF-κB and MAPK signaling pathways, Int. J. Mol. Sci. 20 (5) (2019) 1103, https://doi.org/10.3390/ijms20051103.
[9] Y.-Y. Gu, X.-S. Liu, X.-R. Huang, X.-Q. Yu, H.-Y. Lan, Diverse role of TGF-β in kidney disease, Front. Cell Dev. Biol. 8 (2020) 123, https://doi.org/10.3389/fcell.2020.00123.
[10] L. Gewin, R. Zent, How does TGF-β mediate tubulointerstitial fibrosis?. Seminars in Nephrology Elsevier, 2012, pp. 228–235, https://doi.org/10.1016/j.semnephrol.2012.04.001.
[11] Y.E. Zhang, Non-Smad pathways in TGF-β signaling, Cell Res. 19 (1) (2009) 128–139, https://doi.org/10.1038/cr.2008.328.

[12] T. Claudel, B. Staels, F. Kuipers, The Farnesoid X receptor: a molecular link between bile acid and lipid and glucose metabolism, Arterioscler. Thromb. Vasc. Biol. 25 (10) (2005) 2020–2030, https://doi.org/10.1161/01.ATV.0000178994.21828.a7.
[13] M. Herman-Edelstein, T. Weinstein, M. Levi, Bile acid receptors and the kidney, Curr. Opin. Nephrol. Hypertens. 27 (1) (2018) 56–62, https://doi.org/10.1097/MNH.0000000000000374.
[14] Y. Jiao, Y. Lu, X.-y. Li, Farnesoid X receptor: a master regulator of hepatic triglyceride and glucose homeostasis, Acta Pharmacol. Sin. 36 (1) (2015) 44–50, https://doi.org/10.1038/aps.2014.116.
[15] X.X. Wang, D. Wang, Y. Luo, K. Myakala, E. Dobrinskikh, A.Z. Rosenberg, J. Levi, J.B. Kopp, A. Field, A. Hill, FXR/TGR5 dual agonist prevents progression of nephropathy in diabetes and obesity, J. Am. Soc. Nephrol. 29 (1) (2018) 118–137, https://doi.org/10.1681/ASN.2017020222.
[16] A. Marquardt, S. Ghosh, S. Kohli, J. Manoharan, A. ElWakiel, I. Gadi, F. Bock, S. Nazir, H. Wang, J.A. Lindquist, Farnesoid X receptor agonism protects against diabetic tubulopathy: potential add-on therapy for diabetic nephropathy, J. Am. Soc. Nephrol. 28 (11) (2017) 3182–3189, https://doi.org/10.1681/ASN.2016101123.
[17] S. Li, S. Ghoshal, M. Sojoodi, G. Arora, R. Masia, D.J. Erstad, D.S. Ferriera, Y. Li, G. Wang, M. Lanuti, The farnesoid X receptor agonist EDP-305 reduces interstitial renal fibrosis in a mouse model of unilateral ureteral obstruction, Faseb. J. 33 (6) (2019) 7103–7112, https://doi.org/10.1096/fj.201801699R.
[18] M. Úbeda, M. Lario, L. Muñoz, M.-J. Borrero, M. Rodríguez-Serrano, A.-M. Sánchez-Díaz, R. Del Campo, L. Lledó, Ó. Pastor, L. García-Bermejo, Obeticholic acid reduces bacterial translocation and inhibits intestinal inflammation in cirrhotic rats, J. Hepatol. 64 (5) (2016) 1049–1057, https://doi.org/10.1016/j.jhep.2015.12.010.
[19] P. Schwabl, E. Hambruch, B.A. Seeland, H. Hayden, M. Wagner, L. Garnys, B. Strobel, T.-L. Schubert, F. Riedl, D. Mitteregger, The FXR agonist PX20606 ameliorates portal hypertension by targeting vascular remodelling and sinusoidal dysfunction, J. Hepatol. 66 (4) (2017) 724–733, https://doi.org/10.1016/j.jhep.2016.12.005.
[20] P. Comeglio, S. Filippi, E. Sarchielli, A. Morelli, I. Cellai, F. Corcetto, C. Corno, E. Maneschi, A. Pini, L. Adorini, Anti-fibrotic effects of chronic treatment with the selective FXR agonist obeticholic acid in the bleomycin-induced rat model of pulmonary fibrosis, J. Steroid Biochem. Mol. Biol. 168 (2017) 26–37, https://doi.org/10.1016/j.jsbmb.2017.01.010.
[21] S. Nakanishi, S. Toki, Y. Saitoh, E. Tsukuda, K. Kawahara, K. Ando, Y. Matsuda, Isolation of myosin light chain kinase inhibitors from microorganisms: dehydroaltenusin, altenusin, atrovenetinone, and cyclooctasulfur, Biosci. Biotechnol. Biochem. 59 (7) (1995) 1333–1335, https://doi.org/10.1271/bbb.59.1333.
[22] R. Uchida, H. Tomoda, Y. Dong, S. Omura, Alutenusin, a specific neutral Sphingomyelinase inhibitor, produced by penidltium sp. FO-7436, J. Antibiot. 52 (6) (1999) 572–574, https://doi.org/10.7164/antibiotics.52.572.
[23] B. Andersen, J. Smedsgaard, I. Jørring, P. Skouboe, L.H. Pedersen, Real-time PCR quantification of the AM-toxin gene and HPLC qualification of toxigenic metabolites from Alternaria species from apples, Int. J. Food Microbiol. 111 (2) (2006) 105–111, https://doi.org/10.1016/j.ijfoodmicro.2006.04.021.
[24] B.B. Cota, L.H. Rosa, R.B. Caligiorne, A.L.T. Rabello, T.M. Almeida Alves, C.A. Rosa, C.L. Zani, Altenusin, a biphenyl isolated from the endophytic fungus Alternaria sp., inhibits trypanothione reductase from Trypanosoma cruzi, FEMS Microbiol. Lett. 285 (2) (2008) 177–182, https://doi.org/10.1111/j.1574-6968.2008.01221.x.
[25] Y. Hou, J. Li, J.-C. Wu, Q.-X. Wu, J. Fang, Activation of cellular antioxidant defense system by naturally occurring dibenzopyrone derivatives confers neuroprotection against oxidative insults, ACS Chem. Neurosci. 12 (15) (2021) 2798–2809, https://doi.org/10.1021/acschemneuro.1c00023.
[26] A. Elbermawi, A.R. Ali, Y. Amen, A. Ashour, K.F. Ahmad, E.-S.S. Mansour, A.F. Halim, Anti-diabetic activities of phenolic compounds of Alternaria sp., an endophyte isolated from the leaves of desert plants growing in Egypt, RSC Adv. 12 (38) (2022) 24935–24945, https://doi.org/10.1039/d2ra02532a.
[27] Z. Zheng, Z. Zhao, S. Li, X. Lu, M. Jiang, J. Lin, Y. An, Y. Xie, M. Xu, W. Shen, Altenusin, a nonsteroidal microbial metabolite, attenuates nonalcoholic fatty liver disease by activating the farnesoid X receptor, Mol. Pharmacol. 92 (4) (2017) 425–436, https://doi.org/10.1124/mol.117.108829.
[28] L. Ling, M. Yang, W. Ding, Y. Gu, Ghrelin attenuates UUO-induced renal fibrosis via attenuation of Nlrp3 inflammasome and endoplasmic reticulum stress, Am. J. Tourism Res. 11 (1) (2019) 131. PMCID: PMC6357333.
[29] Y.-H. Lo, S.-F. Yang, C.-C. Cheng, K.-C. Hsu, Y.-S. Chen, Y.-Y. Chen, C.-W. Wang, S.-S. Guan, C.-T. Wu, Nobiletin alleviates ferroptosis-associated renal injury, inflammation, and fibrosis in a unilateral ureteral obstruction mouse model, Biomedicines 10 (3) (2022) 595, https://doi.org/10.3390/biomedicines10030595.
[30] S.W. Chua, A. Cornejo, J. Van Eersel, C.H. Stevens, I. Vaca, M. Cueto, M. Kassiou, A. Gladbach, A. Macmillan, L. Lewis, The polyphenol altenusin inhibits in vitro fibrillization of tau and reduces induced tau pathology in primary neurons, ACS Chem. Neurosci. 8 (4) (2017) 743–751, https://doi.org/10.1021/acschemneuro.6b00433.
[31] G. Efstratiadis, M. Divani, E. Katsioulis, G. Vergoulas, Renal fibrosis, Hippokratia 13 (4) (2009) 224. PMCID: PMC2776335.
[32] X. Mai, J. Shang, Q. Chen, S. Gu, Y. Hong, J. Zhou, M. Zhang, Endophilin A2 protects against renal fibrosis by targeting TGF-β/Smad signaling, Faseb. J. 36 (11) (2022) e22603, https://doi.org/10.1096/fj.202101769R.
[33] Y.-T. Chang, M.-C. Chung, C.-H. Chang, K.-H. Chiu, J.-J. Shieh, M.-J. Wu, Anti-EMT and anti-fibrosis effects of protocatechuic aldehyde in renal proximal tubular cells and the unilateral ureteral obstruction animal model, Pharmaceut. Biol. 60 (1) (2022) 1198–1206, https://doi.org/10.1080/13880209.2022.2088809.
[34] H. Zhao, Y. Dong, X. Tian, T.K. Tan, Z. Liu, Y. Zhao, Y. Zhang, D.C. Harris, G. Zheng, Matrix metalloproteinases contribute to kidney fibrosis in chronic kidney diseases, World J. Nephrol. 2 (3) (2013) 84, https://doi.org/10.5527/wjn.v2.i3.84.
[35] D. Duan, R. Derynck, Transforming growth factor–β (TGF-β)–induced up-regulation of TGF-β receptors at the cell surface amplifies the TGF-β response, J. Biol. Chem. 294 (21) (2019) 8490–8504, https://doi.org/10.1074/jbc.RA118.005763.
[36] A. Nogueira, M.J. Pires, P.A. Oliveira, Pathophysiological mechanisms of renal fibrosis: a review of animal models and therapeutic strategies 31 (1) (2017) 1–22, https://doi.org/10.21873/invivo.11019.
[37] E. Martínez-Klimova, O.E. Aparicio-Trejo, E. Tapia, J. Pedraza-Chaverri, Unilateral ureteral obstruction as a model to investigate fibrosis-attenuating treatments, Biomolecules 9 (4) (2019) 141, https://doi.org/10.3390/biom9040141.
[38] D. Feng, C. Ngov, N. Henley, N. Boufaied, C. Gerarduzzi, Characterization of matricellular protein expression signatures in mechanistically diverse mouse models of kidney injury, Sci. Rep. 9 (1) (2019) 16736, https://doi.org/10.1038/s41598-019-52961-5.
[39] S.S. Soni, D. Cruz, I. Bobek, C.Y. Chionh, F. Nalesso, P. Lentini, M. de Cal, V. Corradi, G. Virzi, C. Ronco, NGAL: a biomarker of acute kidney injury and other systemic conditions, Int. Urol. Nephrol. 42 (2010) 141–150.
[40] Y. Xiong, Y. Chang, J. Hao, C. Zhang, F. Yang, Z. Wang, Y. Liu, X. Wang, S. Mu, Q. Xu, Eplerenone attenuates fibrosis in the contralateral kidney of UUO rats by preventing macrophage-to-myofibroblast transition, Front. Pharmacol. 12 (2021) 620433, https://doi.org/10.3389/fphar.2021.620433.